IEEE Access
Multidisciplinary | Rapid Review | Open Access Journal

Received March 19, 2022, accepted April 9, 2022, date of publication April 13, 2022, date of current version April 20, 2022.

*Digital Object Identifier 10.1109/ACCESS.2022.3167032*

# Joint Digital Analogue DVB-S2(X) Link Optimization in Non-Linear Channel

**MENGWEI SUN[1], (Member, IEEE), GEORGE GOUSSETIS[2], (Senior Member, IEEE), KAI XU[1,2], YUAN DING[2], (Member, IEEE), STEPHEN MCLAUGHLIN[2], (Fellow, IEEE), ANDREA SEGNERI[2,3], AND MARÍA JESÚS CAÑEVATE SÁNCHEZ[2]**

[1]School of Engineering, Institute of Digital Communications, The University of Edinburgh, Edinburgh EH9 3FG, U.K.
[2]School of Engineering and Physical Sciences, Institute of Sensors Signals and Systems, Heriot-Watt University, Edinburgh EH14 4AS, U.K.
[3]Step Over Srl, 00181 Rome, Italy

Corresponding author: Mengwei Sun (msun@ed.ac.uk)

This work was supported in part by the Engineering and Physical Sciences Research Council (EPSRC) (U.K.) under Grant EP/P025129/1, Grant EP/V002635/1, and Grant EP/L020009/1; and in part by the European Union's Horizon 2020 Research and Innovation Program through the Marie Skodowska-Curie Grant REVOLVE 722840.

**ABSTRACT** Future broadband satellite communication (SatCom) systems require a high throughput of data transmission, which calls for operation at higher frequency bands. Adaptive coding and modulation (ACM) technology has been considered as a means to obtain improved performance further at these frequencies. However, the ACM protocols in current DVB-S2 and DVB-S2(X) standards do not take the effects that arise from the non-linear link with memory into account, which is generated by the cascade of a high-power amplifier (HPA) and digital root raised cosine (RRC) filters. This paper first reveals the non-linear characteristics of the SatCom link, and transfers this into an equivalent full-linear link with an additive noise source thanks to the pre-distortion algorithm. Using this equivalent modeling, an approach of selecting/adapting the optimum coding, modulation scheme and associated system configurations for a given channel fading level is proposed. Both simulations and experimental test-bed performance are presented to validate the proposed method.

**INDEX TERMS** DVB-S2/DVB-S2(X), equivalent full-linear link, non-linear system, optimum configurations.

## I. INTRODUCTION

Demands for the high-data-rate satellite communication (SatCom) are dramatically increasing as services evolve from broadcast to broadband [1], [2]. Currently, high throughput SatCom systems have a capacity of about 100 Gbps and next generation systems are targeting unprecedented levels of Terabit/s [3]. Meanwhile, a number of medium and lower Earth orbit constellations under development are targeting to deliver comparable capacities [4], [5]. The aforementioned changes in capacity are underpinned by the transition to higher frequencies (e.g. Ka-, Q/V- and beyond) [5], [6], where larger bandwidths are available.

Atmospheric phenomena associated with the higher frequencies leads to increased losses and more challenging radio signal amplifications. Consequently, traditional uplink power control (UPC) [7], which provides margin at the expense of an oversized RF front-end, is no longer suitable to maintain high spectrum efficiency links. Instead flexibility on the digital configurations was introduced in the 2nd generation digital video broadcasting satellite standard (DVB-S2) ratified in 2005 [8], as a means to optimize spectrum efficiency. These include a wide range of modulation and coding (MODCOD) rates, options for lower roll-off (ROF) factors for the spectrum shaping filters as well as an adaptive coding and modulation (ACM) functionality that enables optimizing the channel coding and modulation on a frame-by-frame basis [9], [10]. As spectrum efficiency is continuing to be a major drive for emerging satellite missions, the extended version of DVB-S2, DVB-S2(X) [11] published in 2014 introduced additional MODCODs for much finer signal to noise (SNR) granularity as well as three additional smaller ROF factors for the digital filters.

The DVB-S2 framework leads to the exploitation of ACM and the development of modem algorithms to mitigate the non-linearity introduced by high power

The associate editor coordinating the review of this manuscript and approving it for publication was Mohamed M. A. Moustafa.

amplifiers (HPAs) [12]. Specifically, the non-linear characteristics of HPAs depend on the input backoff (IBO). Higher IBOs result in less non-linear distortion to the signal waveform at the expense of reduced signal strength [13]. Recognizing the associated trade-off between non-linearity and signal strength has led to the optimization of IBO in light of different modulation schemes [12]. Existing publications have optimized the digital signal processing parameters but overlooked the interaction between the digital and analogue signal processing [11]. For links relying on a practical HPA, the effects of digital and analogue configurations are intertwined. Consequently, achieving the highest spectrum efficiency in practical link scenarios requires coordinated analogue-digital domain optimization. In particular, lower ROF factors of digital root raised cosine (RRC) filters lead to higher baud-rates for a given bandwidth at the cost of higher inter-symbol interference (ISI), such that the trade-off between ROF and baud-rate applies. On the other hand, the ISI associated with a given ROF is strongly linked with the HPA's IBO, as discussed in [14]. However, the simultaneous optimization for the HPA's IBO, filter's ROF and signal's MODCOD that can maximize the spectrum efficiency while guaranteeing the QoS requirement is yet to be developed. Even though machine learning techniques are a way to work around this, the training process is not compatible with real-time operation of ACM.

This paper fills this gap and proposes a deterministic methodology that enables optimizing the analogue and digital signal processing for emerging broadband SatCom missions, and the key contributions are summarized as follows:

- The intertwined effects of the ROF of RRC filters, MODCOD and IBO of a HPA to the BER performance of the non-linear SatCom link are analyzed in Section II. Then, the non-linear SatCom link is transferred to an equivalent full-linear link with an additive noise source in Section III.B.
- Test-bed based experiments are designed and performed to validate the effectiveness and generality of the equivalent full-linear link in Section III.C.
- The adaptive operation of a DVB-S2(X) link for spectrum efficiency maximization is achieved in Section IV by computationally allocating the MODCOD scheme, ROF and IBO operation for a given HPA and the channel condition. The adaptive control schedule can maintain spectral performance close to optimum and guarantee the QoS requirement.

The paper is organized as follows. In Section II, we provide the background including the SatCom link descriptions, the adverse impacts from the non-linearity and ISI. In Section III, the equivalent full-linear link by translating the ISI into an additive Gaussian noise is established, the designed test-bed and the measured results are also provided. In Section IV, the adaptive control schedule specifying the selected combination of the MODCOD, ROF and IBO is proposed. Finally, conclusions are drawn in Section V.

## II. DVB-S2/DVB-S2(X) SATCOM LINK

In this section, we elaborate the end-to-end SatCom link for DVB-S2/DVB-S2(X) standards and investigate the non-linear distortion. The system block diagram of the forward link is shown Fig. 1 [8], [11].

- At the Gateway transmitter (Tx), the mode adaptation is first applied on the input data, which provides input stream interfacing, synchronization, null-packet deletion, etc. Then, the stream adaptation is applied, i.e. padder and base-band (BB) scrambling, followed by the forward error correction (FEC) encoding, consisting of Bose–Chaudhuri–Hocquenghem (BCH) codes, low-density parity check (LDPC) inner codes and bit interleaver which is discussed in Section II.A. The available LDPC rates in DVB-S2 include {1/4, 1/3, 2/5, 1/2, 3/5, 2/3, 3/4, 4/5, 5/6, 8/9, 9/10}. The resulting sequence is then modulated using one of the schemes including QPSK, 8PSK, 16APSK and 32APSK in the DVB-S2 standard [8], and 64APSK, 128APSK and 256APSK modulation schemes are added in the extended DVB-S2(X) standard [11]. In this paper, we focus on the 16APSK modulation elaborated in Section II.B. The physical layer frame is then applied to the modulated signal, synchronous with the FEC frames. Finally, an RRC filter is applied before the up-conversion for transmitting to satellite transponders through the uplink/feeder link.
- An HPA is equipped at the satellite transponder to amplify the signals received from the uplink and then the amplified signals are relayed to the receiver on the ground through the downlink/user link. The details of the HPA characteristic are discussed in Section II.C. As pointed out by the DVB-S2 working group, the downlink noise dominates the overall link thermal noise and can be assumed as additive white Gaussian noise (AWGN) [8], [11].
- At the receiver end (Rx), i.e. the ground users/terminals, a matched RRC filter is applied after frequency down-conversion and digital sampling, then followed by base-band signal demodulation and decoding. Output signals from the matched RRC, i.e. signals at Point B in Fig. 1, suffer from the distortion which is classified into warping and clustering [12]. The factors affecting the distortion are elaborated in Section II.B to Section II.E.

### A. FEC CODE

The LDPC-based FEC concatenated with BCH codes are applied in the DVB-S2(X) system which is very powerful to improve the BER performance [11], [15]. The FEC and modulation order may be changed across different frames when an ACM is used, but remains constant within a frame. Fig. 2 indicates the mapping relations between the input and output BER of the BCH decoder with different LDPC code-rate and the 16APSK modulation [16], [17]. For example, the FEC is able to improve BER performance from 0.02 to as low

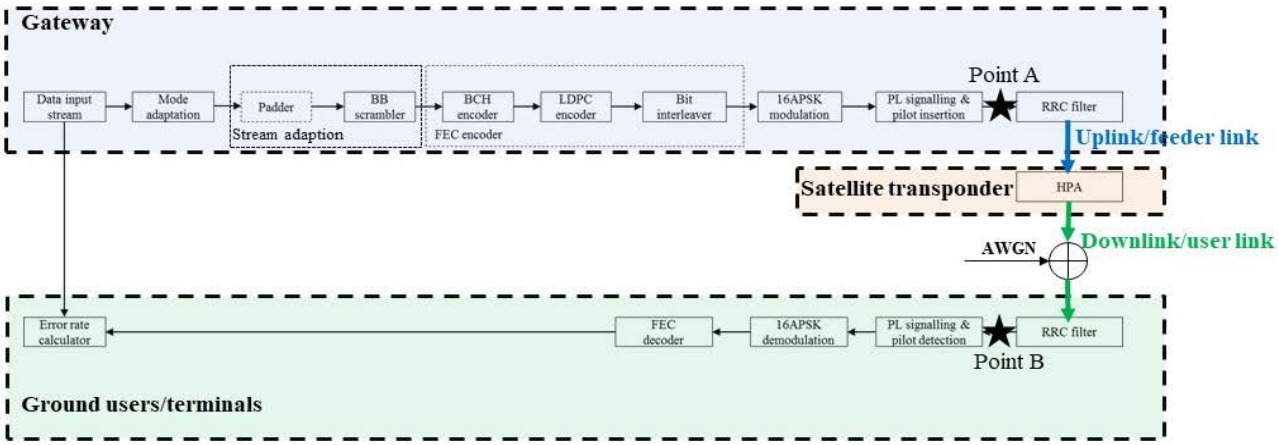


**FIGURE 1.** Block diagram of the DVB-S2/DVB-S2(X) link from gateway, through satellite transponder, to ground terminal.

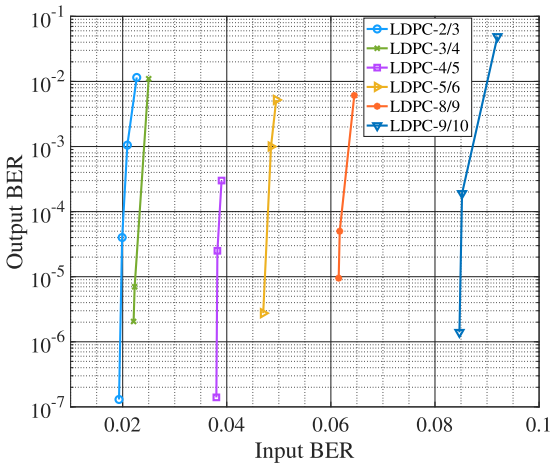


**FIGURE 2.** BER mappings between systems with FEC and without FEC for various LDPC code rates.

as $10^{-4}$ by applying LDPC-9/10. The LDPC code efficiency for error correction becomes greater with the decreasing of the code rate, while leads to lower spectrum efficiency.

### B. MODULATION SCHEMES

APSK modulation schemes are used in DVB-S2 and DVB-S2(X) standards as their circular symmetry constellation diagrams are particularly suited to combat the non-linear effects of HPAs [18], [19]. The constellation of the 16APSK modulation focused in this paper is composed of two concentric rings of uniformly spaced 4 and 12 PSK points, respectively [8], as the reference points shown in Fig. 3. The modulated constellation symbol set is $\mathcal{S} := \{s_0, \ldots, s_{M-1}\}, M = 16$. The ratio of the outer circle radius $R_2$ to the inner circle radius $R_1$ is denoted as $\lambda = R_2/R_1$. The average symbol energy of the 16APSK is calculated as

$$E_s = (R_1^2 + 3R_2^2)/4 = (1 + 3\lambda^2)R_1^2/4. \tag{1}$$

To facilitate analysis in this paper, $E_s$ is normalized to be unity. We note that although the analysis presented in this

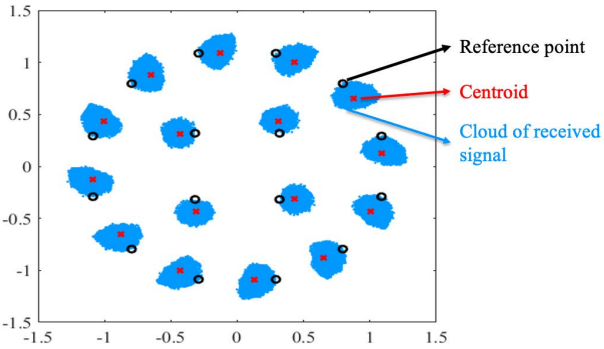


**FIGURE 3.** Distortion phenomenon of the signal at Point B in Fig. 1 system: warping and clustering.

paper is based on the 16APSK modulation, but it can be readily adapted for other APSK modulations.

### C. HPA AT THE SATELLITE TRANSPONDER

The non-linear amplification characteristic of the satellite HPA defined in DVB-S2(X) is adopted and analyzed in this paper. The HPA is constructed using the Saleh's model [8], [20]. The compression of signal power level is characterized as AM/AM effect, see (2), and the relationship between input power level and output phase rotation is characterized by AM/PM effect, see (3).

$$A_{AM/AM}[u] = \frac{a_A u}{1 + b_A u^2}, \tag{2}$$

$$\Phi_{AM/PM}[u] = \frac{a_\Phi u^2}{1 + b_\Phi u^2}. \tag{3}$$

Here, $u$ denotes the magnitude of the input signal, and the coefficient values $a_A = 2.1322$, $b_A = 1.0746$, $a_\Phi = 1.70$, $b_\Phi = 1.5072$ are taken from [21]. The nonlinear characteristics of the HPA, i.e. AM/AM compression and AM/PM rotation, cause the constellation centroids of the received signals to no longer be lying on the top of the reference points. This effect is referred to warping distortion and is shown in Fig. 3. From Fig. 3, we can see that the warping distortion

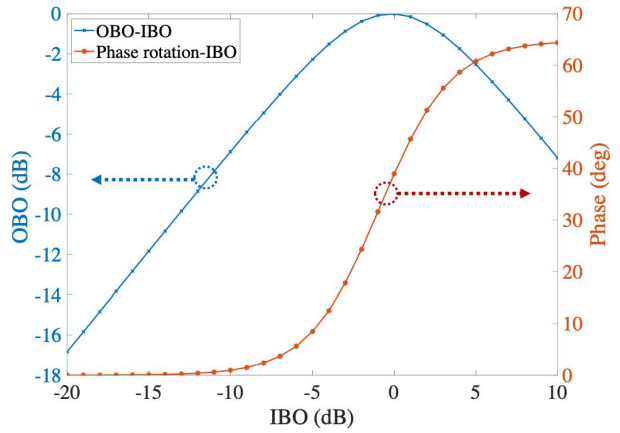


**FIGURE 4. OBO-IBO and phase rotation-IBO characteristics of the specified HPA in DVB-S2(X).**

of the outer ring points, i.e. the points with larger amplitude, is more distinct than the inner ring points, i.e. the points with smaller amplitude.

The IBO of a HPA (in dB) is defined as $\beta = 10\log_{10}(P_{avg}/P_{sat})$, indicating the deviation of the average input power $P_{avg} = |u|^2$ from the input saturation power $P_{sat}$. Smaller values of $\beta$ indicate higher IBO. The output back-off (OBO) is a function of IBO. Fig. 4 illustrates the non-linear OBO-IBO and phase rotation-IBO behaviors. Higher IBO results in reduced non-linear HPA distortions at the cost of lower output power and DC power efficiency.

### D. RRC FILTERS

Raised-cosine (RC) filters are widely used in digital systems for pulse-shaping [22]. Usually the RC filter is split equally into a pair of RRC filters, with one at the Tx, and the other at the Rx. They perform matched filtering to optimize the signal to noise ratio (SNR) in the presence of additive channel noise [23], [24]. The impulse response of an RRC filter in time-domain is [22]

$$h_{RRC}(t) = \frac{2\gamma}{\pi\sqrt{T}} \frac{\cos\left[(1+\gamma)\pi t/T\right] + \frac{\sin[(1-\gamma)\pi t/T]}{4\gamma t/T}}{1-(4\pi t/T)^2}, \quad (4)$$

where $\gamma$ represents the ROF, $f$ represents the frequency and $T$ is the sampling period. The spectrum efficiency of a communication system is defined as the ratio between the bit rate $R_b$ and the transmission bandwidth [25]. Therefore, for a given $R_b$, smaller $\gamma$ gives higher spectrum efficiency due to narrower bandwidth. However, the capability of suppression in stop bands is reduced [22].

Note, RRC filters are theoretically infinite impulse response (IIR) filters. However, they are implemented as finite impulse response (FIR) filters in practice since FIR filters are intrinsically stable and use less hardware resources. The number of FIR filter taps is given as $N_{tap} = D \times M_{sam}$, where $D$ defines the number of symbols spanned by the impulse response of the filter and $M_{sam}$ is the amount of up-sampling, $D$ and $M_{sam}$ are both integers. Therefore, the impulse response of IIR-RRC filter is written as

$$\begin{aligned} h_{IIR-RRC} &= h_{FIR-RRC} + \Delta h_{RRC}, \\ &= \sum_{t=\bar{t}} h_{RRC}(t) + \sum_{t=\underline{t}} h_{RRC}(t), \end{aligned} \quad (5)$$

where $\bar{t} = \left[-\frac{DT}{2} : \frac{T}{M_{sam}} : \frac{DT}{2}\right]$ and $\underline{t} = \left(-\infty : \frac{T}{M_{sam}} : -\frac{DT}{2}\right) \cup \left(\frac{DT}{2} : \frac{T}{M_{sam}} : \infty\right)$. From (5) we can see that two cascaded FIR RRC filters, as shown in Fig. 5(a), cannot represent an ideal RC filter response. Specifically, the output signals from the Rx RRC, i.e. Point B in Fig. 5(a), are derived as

$$\begin{aligned} &S \otimes h_{FIR-RRC} \otimes h_{FIR-RRC}, \\ &= S \otimes (h_{IIR-RRC} - \Delta h_{RRC}) \otimes (h_{IIR-RRC} - \Delta h_{RRC}), \\ &= S \otimes h_{IIR-RRC} \otimes h_{IIR-RRC} \\ &\quad + [S \otimes \Delta h_{RRC} \otimes \Delta h_{RRC} - 2\, S \otimes h_{IIR-RRC} \otimes \Delta h_{RRC}], \\ &= S \otimes h_{RC} + S_{ISI}. \end{aligned} \quad (6)$$

Here, $\otimes$ represents the convolution operation, $S$ is the modulated signals at the transmitter end, and the ISI introduced by the concatenation of two matched FIR RRCs is denoted as $S_{ISI}$.

The constellations of the output signals at Point B for different ROF values are shown in Fig. 5(b), which indicate that the resulting ISI is a nearly circularly symmetric complex Gaussian spreading and can be approximated by a complex Gaussian distribution with zero mean. Moreover, the simulated results of the complex Gaussian spreading variance are shown in Fig. 5(c), which indicate that the variance is dependent on $\gamma$, $M_{sam}$ and $D$. From this plot, we can observe that a larger $D$ gives a better approximation to the ideal response, and the ISI is not monotonic versus $\gamma$ but fluctuates with a decreasing trend. Furthermore, $M_{sam}$ has little impact on the filter performance other than to reduce the variation in stop band attenuation for small changes in $D$ or $\gamma$. Following DVB-S2(X) standard and for the ease of comparison with some previous works, the RRCs are implemented with $N_{tap} = 80$, $M_{sam} = 8$ and $D = 10$ in our study [26].

### E. INTERACTION BETWEEN DIGITAL AND ANALOGUE SIGNAL PROCESSING

The insertion of the non-linear HPA between two RRC filters, as shown in Fig. 1, results in the mismatch of the receiver RRC filter to the Rx signal. Therefore, the uncertainty caused by the ISI doesn't follow Gaussian spreading any more, but in irregular shapes as shown in Fig. 3, which is called clustering. Note, the resulting clustering is the energy exchange between transmitted signals, which is related to both the amplitude of current signal and the amplitudes of neighboring signals, in a statistical sense, consist of all 16 symbols with equal probability. Due to the equal probability of the neighboring symbols, the clustering effect is independent of magnitude of symbols currently transmitted. Hence, there is no distinct differences of the spreading between the inner-ring points

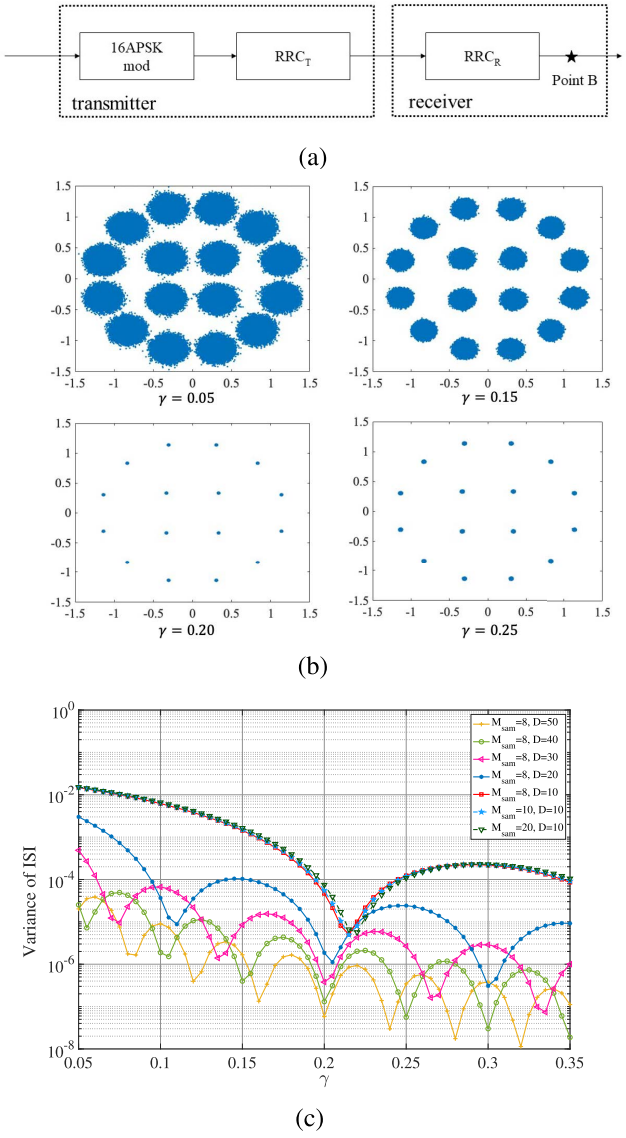


**FIGURE 5.** ISI caused by two cascaded FIR RRC filters. (a) Link model. (b) Signal constellations at the output of receiving RRC. (c) Equivalent variance of ISI versus $\gamma$ under different up-sample $M_{sam}$ and memory span values $D$.

and outer-ring points in Fig. 3. Overall, the combination of the HPA with two matched RRC filters leads to a non-linear SatCom link with memory and results in the signals at Point B in Fig. 1 suffering from warping and clustering distortions. The distortions in turn lead to significant degradation of QoS performance, making the existing propagation impairments mitigation techniques (PIMTs) inefficient.

## III. DIGITAL PRE-DISTORTION ALGORITHM AND EQUIVALENT FULL-LINEAR LINK

Digital pre-distortion algorithms commonly rely on iterative numerical optimization techniques [27], [28]. In this section, a digital pre-distortion algorithm is firstly introduced. With the pre-distortion applied before the transmitter RRC filter, see Point A in Fig. 1, the warping and clustering effects can be

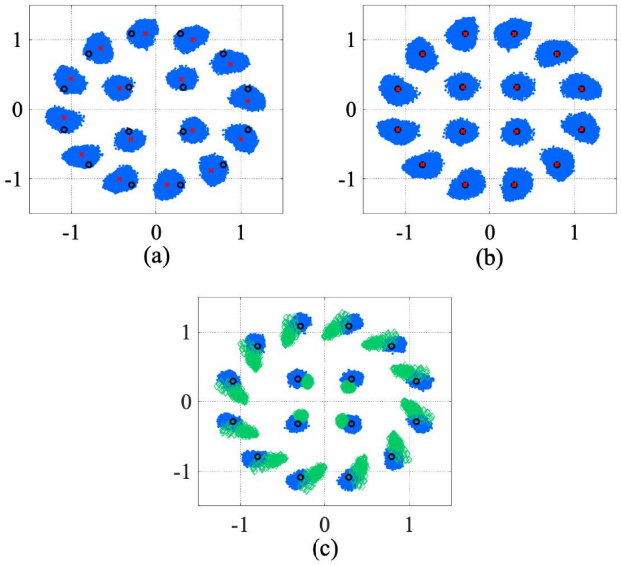


**FIGURE 6.** The illustration of the digital pre-distortion algorithm. (a) Output signal without pre-distortion. (b) Output signal with only coarse pre-distortion. (c) Output signal with pre-distortion represented in blue points and the green squares are the pre-distortion constellation mappings.

significantly suppressed and the reduced ISI can be approximated as an equivalent addictive Gaussian noise. Hence, the non-linear link can then be transferred to an equivalent full-linear link with an additive noise source. In order to validate the effectiveness of the pre-distortion algorithm and the equivalent linear link, a DVB-S2(X) test-bed at intermediate frequency (IF) is designed and implemented, and the experimental results are presented at the end of this section.

### A. DIGITAL PRE-DISTORTION

The pre-distortion used in this paper consists of two main steps, coarse and refined pre-distortion [12], [28], [29]. The coarse pre-distortion is designed to overcome the wrapping distortion, i.e. minimizing the error signal using an interactive least mean square (LMS) method. The output constellation of the coarse pre-distortion is shown in Fig. 6(b). The refined pre-distortion is then followed to combat the clustering effects, i.e. conditioning the pre-distorted modulator constellation not only to the current transmitted symbol but also to the $(L-1)/2$ preceding and $(L-1)/2$ following symbols ($L$ symbols in total and $L$ is odd). Therefore, for the current received symbol, there are $M^{L-1}$ combinations of neighboring symbols. In this paper, $M = 16$ for 16APSK, and $L$ is set to be 3, i.e. one preceding and one following neighboring symbols are considered. Hence, one constellation cloud consists of $M^2$ sub-clouds and there are $M^3$ sub-clouds when all $M$ constellations are considered. The goal of refined pre-distortion is to minimize the error signal between the centroid of each sub-cloud with the correspond reference point. The result achieved by the pre-distortion is a look-up table specifying the output constellation mappings which can be represented as a 3D matrix, as the green squares shown in

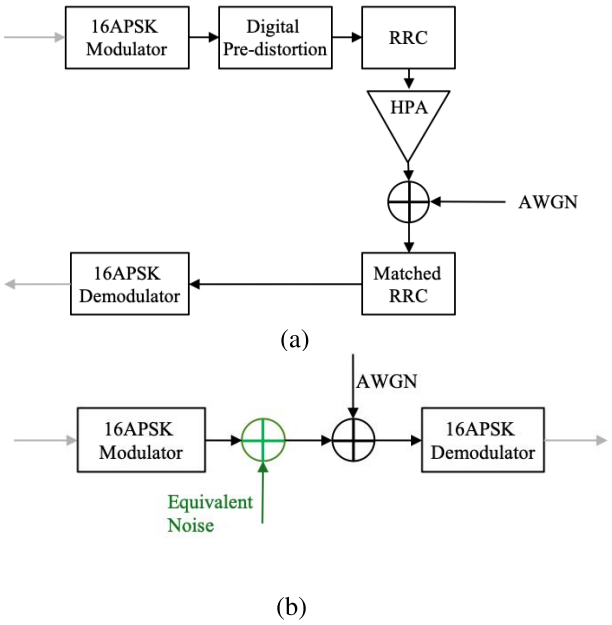


**FIGURE 7.** (a) Non-linear link with HPA and two RRC filters. (b) Equivalent full-linear link with extra additive noise source.

Fig. 6(c). The modulator reads the look-up table in real-time with an address determined by the preceding, the current and the following symbols. The blue points in Fig. 6(c) are the output constellation after the matched RRC with the digital pre-distortion.

### B. EQUIVALENT GAUSSIAN NOISE OF ISI WITH PRE-DISTORTION

By applying the pre-distortion algorithm, the warping effect caused by the nonlinear characteristic of the HPA is largely overcome, and the clustering effect due to the ISI is reduced and can be approximated by an equivalent Gaussian noise. Then, the non-linear link, see Fig. 7(a), is equivalent to a full-linear link with an additive noise source, see Fig. 7(b). The mean of the additive noise is zero, and its variance $\sigma^2_{\text{ISI}}$ is obtained with a Monte-Carlo simulation and calculated as

$$\sigma^2_{\text{ISI}} = \frac{\sum_{n=1}^{N}\sum_{m=0}^{M-1}(y_n - s_m)^2\delta(x_n, s_m)}{N-1}, \tag{7}$$

where $x_n$ represents $n$-th modulated signal, $x_n \in \mathcal{S}$. $N$ is the length of modulated signals. $\delta(x_n, s_m) = 1$ if and only if $x_n = s_m$, otherwise, $\delta(x_n, s_m) = 0$. $y_n$ represents the signals after the Rx RRC with pre-distortion. The obtained variance values are summarized in Table 1 as functions of the ROF $\gamma$ and IBO $\beta$. From this table, we can see that the equivalent variance reduces as $\beta$ decreases, as the non-linearity of the HPA becomes less distinct. However, there is a floor owing to the imperfect RRC characteristic as shown in Fig. 5.

The achieved equivalent noise in Table 1 is validated by comparing the BER performance under the two links in Fig. 7. The numerical results are shown in Fig. 8, in which the BER curves under these two links show good agreement. We can also see the significant improvement of system performance

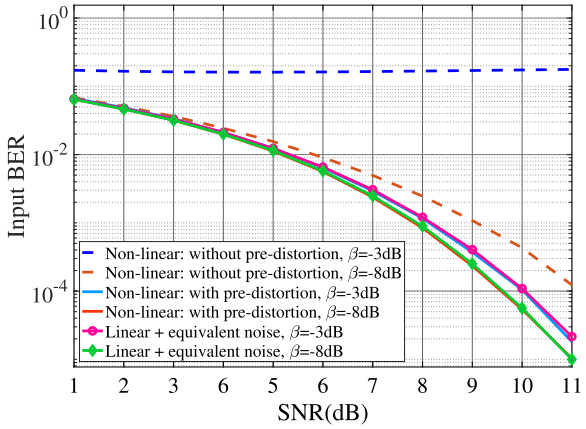


**FIGURE 8.** BER performance comparison between non-linear link with/without pre-distortion and the equivalent linear link with additive noise source, $\gamma = 0.35$, specified HPA in DVB-S2(X).

relying on the pre-distortion algorithm. For example, for a higher IBO value, i.e. $\beta = -3$dB, the input BER can be suppressed down to approximately $10^{-5}$ for moderate SNRs, while an SNR gain of 1.5 dB can be achieved by the pre-distortion method for a lower IBO value, i.e. $\beta = -8$dB, when the BER $= 10^{-4}$.

### C. TEST-BED BASED EXPERIMENTS FOR PRE-DISTORTION AND EQUIVALENT FULL-LINEAR LINK VALIDATION

The equivalent full-linear link is validated in this section experimentally. The amplifier ZJL-4HG+ from Mini-Circuits operating at 2.4GHz operation is used in the test-bed. The AM/AM behavior is modeled as the Bessel-Fourier considering the accuracy in all operating regions. The Bessel-Fourier model consists on a particular kind of generalized Fourier series based on Bessel functions of the first kind $J_1(\cdot)$ [30], [31]

$$B_{AM/AM}(\mu) = \sum_{m=1}^{M_J} c_m J_1(v_1 m\mu), \tag{8}$$

where $\mu$ denotes the magnitude of the input signal, $M_J$ is the number of terms of the Bessel series with assigned coefficients $\{c_m\}_{m=1}^{M_J}$ and $v_1$ is another coefficient. The main advantage of the Bessel-Fourier model is the extensibility, in the sense that the number of Bessel series can be increased for improved model accuracy, and in this paper, the number is set to be $M_J = 23$ and the coefficient $v_1 = 16.006$. The measured AM/AM conversion of the selected HPA and the fitted AM/AM conversion using the Bessel-Fourier behavioral model are depicted and compared in Fig. 9. We note that the selected solid state amplifier has negligible AM/PM non-linearity and hence this is not plotted.

Based on the two-step pre-distortion algorithm, the pre-distortion look-up table for amplifier ZJL-4HG+ is generated through Monte-Carlo simulation. Then, the experimental test-bed is set up as Fig. 10, which measures the BER performance of un-coded 16APSK signal for different

**TABLE 1.** Equivalent noise variance $\sigma^2_{ISI}$ for different IBO and ROF, specified HPA in DVB-S2(X).

| IBO $\beta$(dB) | $\gamma = 0.05$ | $\gamma = 0.10$ | $\gamma = 0.15$ | $\gamma = 0.20$ | $\gamma = 0.25$ | $\gamma = 0.35$ |
|---|---|---|---|---|---|---|
| **0** | 0.0497 | 0.0368 | 0.0267 | 0.0210 | 0.0175 | 0.0113 |
| **−1** | 0.0303 | 0.0191 | 0.0139 | 0.0092 | 0.0076 | 0.0038 |
| **−2** | 0.0240 | 0.0143 | 0.0083 | 0.0054 | 0.0041 | 0.0019 |
| **−3** | 0.0194 | 0.0110 | 0.0053 | 0.0029 | 0.0025 | 0.0014 |
| **−4** | 0.0176 | 0.0086 | 0.0038 | 0.0019 | 0.0015 | 7.3598e-04 |
| **−5** | 0.0162 | 0.0075 | 0.0026 | 0.0011 | 7.2893e-04 | 4.6501e-04 |
| **−6** | 0.0155 | 0.0069 | 0.0021 | 5.4797e-04 | 4.1060e-04 | 2.5624e-04 |
| **−7** | 0.0152 | 0.0065 | 0.0017 | 2.4809e-04 | 2.5297e-04 | 1.4992e-04 |
| **−8** | 0.0152 | 0.0063 | 0.0016 | 1.3410e-04 | 2.0919e-04 | 1.1771e-04 |
| **−9** | 0.0151 | 0.0063 | 0.0015 | 9.6810e-05 | 1.4992e-04 | 9.9372e-05 |
| **−10** | 0.0152 | 0.0063 | 0.0015 | 6.1416e-05 | 1.3895e-04 | 9.3706e-05 |
| **−11** | 0.0151 | 0.0063 | 0.0015 | 5.5189e-05 | 1.3120e-04 | 8.8208e-05 |
| **−12** | 0.0151 | 0.0063 | 0.0015 | 4.9254e-05 | 1.2706e-04 | 8.7422e-05 |

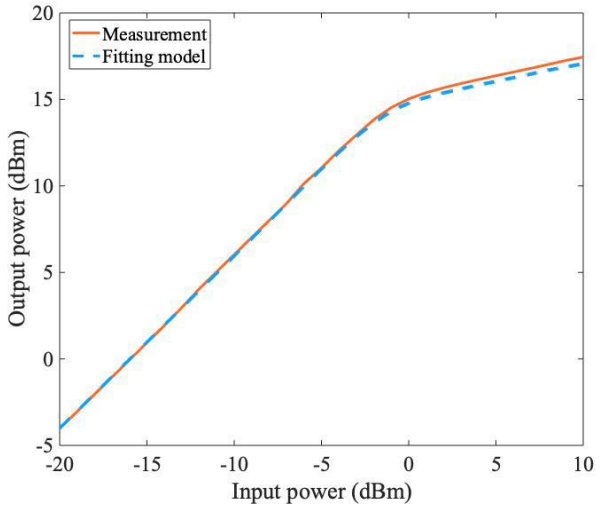


**FIGURE 9.** Measured and fitted Bessel-Fourier AM/AM conversions of the power amplifier ZJL-4HG+ from Mini Circuits.

IBO levels and SNRs at the presence of the HPA and a pair of RRC filters. Specifically, the modulated source signals with the pre-distortion are firstly generated in MATLAB. Then, in order to generate the signals for transmission, the filtered symbols at the output of the transmit RRC filter are converted into I16 format and recorded into a binary file, before being translated into waveforms in the vector signal generator (VSG). A driver is connected between the VSG and the device under test (DUT) to keep the HPA input signal as linear as possible [30]. The output of the HPA is connected with a fixed attenuator and a variable attenuator to adjust the SNR value of the link, as shown in Fig. 10(b). The received data is recorded as a binary file by the vector signal analyzer (VSA). Finally, the received data is processed by the matched RRC filter and then demodulated in MATLAB.

The parameters and the corresponding values used in this section are listed in Table 2. Based on the digital pre-distortion in Section III.A, the variance of the additive Gaussian noise for the equivalent linear link approximating the non-linear link depicted in Fig. 10(a) is obtained with Monte-Carlo simulations, and listed in Table 3.

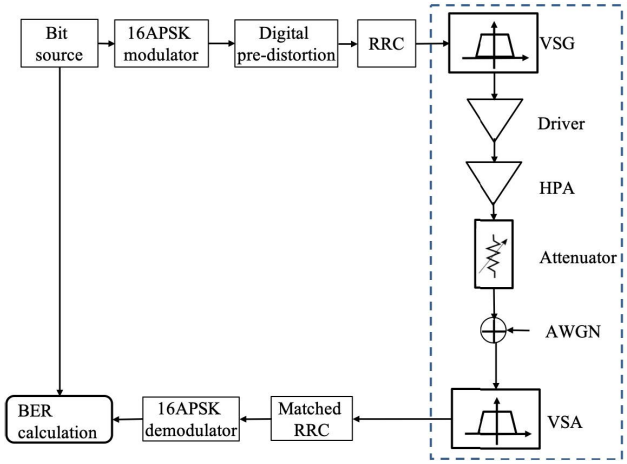


**FIGURE 10.** Test-bed implemented. (a) Block diagram for measuring the BER performance of un-coded digital 16APSK signals. (b) Experimental setup with HPA devices whose AM/AM conversion is depicted in Fig. 9.

The comparisons of the simulated BER performance between the non-linear link with pre-distortion and the equivalent linear link with additive noise source are shown in Fig. 11, and exhibit good agreement. The comparisons between the measured BER and the simulated BER performance are shown

**TABLE 2. Configuration of the parameters for simulation and measurement platform.**

| Parameter | Value |
|---|---|
| Bandwidth | 480kHz |
| Symbol rate | $3 \times 10^6$ symbols/second |
| Frame length | 400 symbols |
| Roll-off factor | 0.35 |
| RRC filter span | 10 symbols |
| RRC filter gain | $\sqrt{8}$ |
| Up-sampling factor | 8 samples/symbol |

**TABLE 3. Equivalent noise variance for the power amplifier ZJL-4HG+ under ROF $\gamma = 0.35$.**

| IBO $\beta$ (dB) | 0 | -2 | -4 | -8 |
|---|---|---|---|---|
| Variance | 0.0026 | 0.0020 | 0.0010 | 2.3066e-04 |

in Fig. 12. From this figure, we can see that for higher IBO values, e.g. $\beta = 0$dB, the application of the pre-distortion algorithm can improve the BER performance significantly, while for lower IBO value, i.e. $\beta = -8$dB, the performance without pre-distortion comes closest to the performance with pre-distortion, which implies that the operation is in the HPA linear region. Furthermore, it can also be observed that the simulated and measured BER values are in good overall agreement. The reason for the measured BER curves being slightly higher than the simulated curves relies on the fact that extra noise is inevitable in the test-bed, and also in simulations, perfect synchronization is assumed while this is not the case in the test-bed measurement.

## IV. ADAPTIVE OPERATION OF DVB-S2X LINK

Based on the equivalent full-linear link with additive noise source, an adaptive operation which can jointly optimize the IBO, ROF, MODCOD is proposed in this section. The target of the link optimization is to maximize the spectrum efficiency of SatCom links while maintaining the required QoS performance, e.g. below a specific maximum allowable BER. This is a multi-dimensional optimization problem, involving three system parameters, i.e. MODCOD, RRC ROF, and IBO of the given HPA, and is also influenced by the channel noise power. The optimization problem is mathematically formulated in (9) and (10),

$$\max E(\alpha, \gamma) \tag{9}$$

$$\text{s.t. } B(\alpha, \gamma, \beta, N_0) \leq \tau. \tag{10}$$

Here, $E$ represents the spectrum efficiency determined by the MODCOD scheme $\alpha$ and ROF $\gamma$. $B$ represents the BER determined by $\alpha, \gamma$, IBO value $\beta$ and channel noise power $N_0$. $\tau$ denotes the input BER threshold of the required detection performance. Note, $\beta$ has impact only on the BER but no effect on the spectral efficiency. Therefore, the optimum IBO value which can minimize the input BER is firstly obtained.

### A. OPTIMUM IBO FOR DIFFERENT ROF VALUES

The optimum IBO for the minimal input BER value can be determined by minimizing the total link degradation denoted

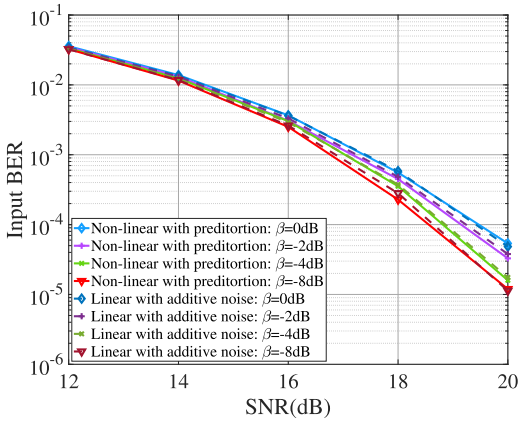


**FIGURE 11. Comparison between non-linear link with pre-distortion and equivalent linear link with additive noise source, $\gamma = 0.35$, power amplifier ZJL-4HG+.**

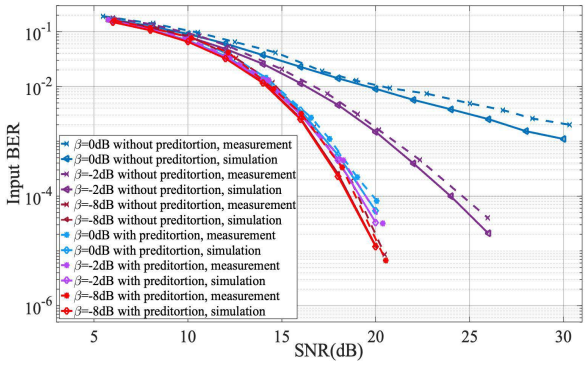


**FIGURE 12. Comparison between simulated and measured BER with/without the pre-distortion algorithm for un-coded 16-APSK in AWGN channel, $\gamma = 0.35$, power amplifier ZJL-4HG+.**

as $D_{tot}$, see the derivation in Appendix. $D_{tot}$ is defined as the sum of the link degradation and the HPA OBO [12]

$$D_{tot}[\text{dB}] = \left\{ \left[\frac{E_s}{N_0}\right]_{\text{ref}}^{\text{NL}} - \left[\frac{E_s}{N_0}\right]_{\text{ref}}^{\text{AWGN}} - \xi \right\} [\text{dB}], \tag{11}$$

where $\left[\frac{E_s}{N_0}\right]_{\text{ref}}^{\text{NL}}$ and $\left[\frac{E_s}{N_0}\right]_{\text{ref}}^{\text{AWGN}}$ are the average symbol energy over noise density required to achieve the target BER in the non-linear and linear channels, respectively. $\xi$ denotes the value of OBO in dB which is a negative constant as shown in Fig. 4. By approximating the ISI as additive noise, the relation between the required average symbol energy for non-linear and linear links can be written as

$$\frac{[E_s]_{\text{ref}}^{\text{NL}}}{\sigma_{\text{ISI}}^2 + N_0} = \frac{[E_s]_{\text{ref}}^{\text{AWGN}}}{N_0}. \tag{12}$$

Then, the required energy over noise density in a non-linear channel can be presented as

$$\left[\frac{E_s}{N_0}\right]_{\text{ref}}^{\text{NL}} = \left[\frac{E_s}{N_0}\right]_{\text{ref}}^{\text{AWGN}} \left(1 + \frac{\sigma_{\text{ISI}}^2}{N_0}\right). \tag{13}$$

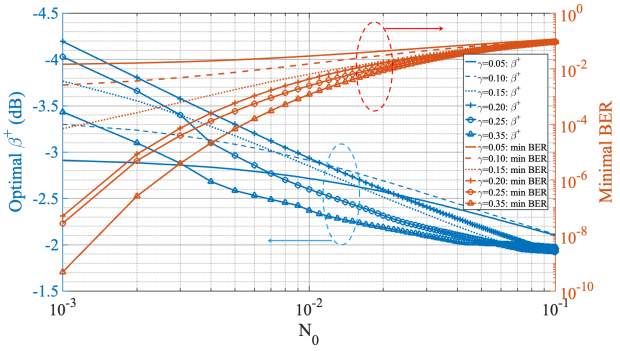


**FIGURE 13.** Optimum IBO $\beta^{\dagger}$ for different $\gamma$ with varied AWGN power density $N_0$, specified HPA in DVB-S2(X).

And in dB format, it is

$$\left\{\left[\frac{E_s}{N_0}\right]_{\text{ref}}^{\text{NL}} - \left[\frac{E_s}{N_0}\right]_{\text{ref}}^{\text{AWGN}}\right\}[\text{dB}] = \left(1 + \frac{\sigma_{\text{ISI}}^2}{N_0}\right)[\text{dB}]. \quad (14)$$

Therefore, $D_{tot}$ can be rewritten as

$$D_{tot} = \left\{\left(1 + \frac{\sigma_{\text{ISI}}^2}{N_0}\right) - \xi\right\}[\text{dB}]. \quad (15)$$

As mentioned previously, the equivalent variance $\sigma_{\text{ISI}}^2$ and $\xi$ are both functions of IBO, i.e. $\sigma_{\text{ISI}}^2 = f(\beta)$ and $\xi = g(\beta)$. Then, the optimum IBO denoted as $\beta^{\dagger}$ for the best BER performance can be obtained by minimizing $D_{tot}$ as below

$$\begin{aligned}\beta^{\dagger} &= \arg\min_{\beta}\{D_{tot}\}, \\ &= \arg\min_{\beta}\left\{\log\left[1 + \frac{f(\beta)}{N_0}\right] - \log\left[g(\beta)\right]\right\}. \quad (16)\end{aligned}$$

The numerical results of the optimum IBO values with the associate BER for different ROF $\gamma$ and channel AWGN power $N_0$ are shown in Fig. 13. From this figure, the optimum IBO $\beta^{\dagger}$ decreases as the link noise power reduces. This is because the signal distortion caused by HPA dominates the detection error when $N_0$ is small. Therefore, $\beta$ should be reduced to make the HPA to work in a more linear region. It can be concluded from Fig. 2 that the impact from FEC codes to the BER performance is monotonic, i.e. the output BER reduces when decreasing the input BER. Therefore, the optimum IBO obtained for the minimal input BER in Fig. 13 is still valid for the output BER with FEC coding.

### B. OPTIMUM DVB-S2(X) LINK CONFIGURATIONS

The adaptive operation is implemented by adjusting the MODCOD scheme and ROF value subject to a certain channel noise power, which is summarized as Algorithm I in Table 4. The improved spectrum efficiency of the proposed algorithm is validated by comparing the spectrum efficiency of the ACM with fixed IBO value $\beta = -5$dB. For example, the output BER threshold (i.e. with FEC) is set to be $10^{-5}$, the input BER thresholds for different MODCOD schemes denoted as $\tau$ are obtained from the curves in Fig. 2 are:

**TABLE 4.** Algorithm I – Adaptive operation of system parameters chose.

- Set the detection performance threshold based on the standard requirement.
- Calculate the input BER thresholds (without FEC) for different MODCOD based on mapping relations shown in Fig. 2.
- Get the real-time channel noise power.
- **For** $\gamma := \{0.05, 0.10, 0.15, 0.20, 0.25, 0.35\}$.
  - Get the minimal BER and the associate optimum IBO obtained in Fig. 13,
  - Get the viable MODCOD schemes by comparing the minimal BER with the input BER thresholds,
  - Calculate the spectral efficiency of each viable MODCOD scheme,
  - Select the optimum MODCOD scheme which responds to the maximum spectral efficiency for each ROF.
- **End For**
- Get the optimal combination of ROF (respond to the optimal IBO) and MODCOD scheme by comparing the spectral efficiency achieved for each ROF.

**TABLE 5.** BER performance comparisons.

| ROF $\gamma$ | Proposed algorithm | | ACM $\beta = -5$dB |
|---|---|---|---|
| | $\beta^{\dagger}$dB | $BER_m$ | $BER_{ACM}$ |
| **0.05** | -3.145 | 0.0435 | 0.0489 |
| **0.10** | -3.38 | 0.0306 | 0.0348 |
| **0.15** | -3.03 | 0.0182 | 0.0303 |
| **0.20** | -3.19 | 0.0163 | 0.0289 |
| **0.25** | -2.63 | 0.0116 | 0.0283 |
| **0.35** | -2.375 | 0.0085 | 0.0280 |

- $\{\ \alpha = 16\text{APSK-}2/3,\ \tau = 0.085\ \}$,
- $\{\ \alpha = 16\text{APSK-}3/4,\ \tau = 0.059\ \}$,
- $\{\ \alpha = 16\text{APSK-}4/5,\ \tau = 0.047\ \}$,
- $\{\ \alpha = 16\text{APSK-}5/6,\ \tau = 0.038\ \}$,
- $\{\ \alpha = 16\text{APSK-}8/9,\ \tau = 0.022\ \}$,
- $\{\ \alpha = 16\text{APSK-}9/10,\ \tau = 0.020\ \}$.

When the channel noise power, for example, is set to be $N_0 = 10^{-2}$, the optimum IBO $\beta^{\dagger}$ and the associated minimal BER $BER_m$ for each ROF $\gamma$ are obtained from Fig. 13, and the BER comparisons between the proposed algorithm and the ACM with $= -5$dB are shown in Tabel 5.

Then, taking $\gamma = 0.05$ for example, only three MODCOD schemes for the proposed algorithm can be chosen, i.e. 16APSK-2/3, 16APSK-3/4 and 16APSK-4/5. This is because for other MODCOD schemes, the BER requirement cannot be met, i.e. $BER_m > \tau$. Finally, 16APSK-4/5 is selected under $\gamma = 0.05$ for the highest spectrum efficiency among the three optional MODCOD schemes. Accordingly, we can achieve the optimum combinations of MODCOD and IBO for each ROF value of the proposed algorithm under $N_0 = 10^{-2}$, and the optimum MODCOD for each ROF value of the ACM under $N_0 = 10^{-2}$, as listed in Table 6. Based on Table 5 and Table 6, the maximum spectrum efficiency of the proposed algorithm under $N_0 = 10^{-2}$ is 3.1020 with the input BER $BER = 0.0182$, and the optimal combination of link parameters is $\{\ \alpha = 16\text{APSK-}9/10,\ \gamma = 0.15,\ \beta^{\dagger} = -3.03\text{dB}\ \}$. By contrast, the maximum spectral efficiency of the ACM with fixed IBO $\beta = -5$dB under $N_0 = 10^{-2}$ is 3.002 with

**TABLE 6. Spectral efficiency for different MODCOD and ROF under $N_0 = 10^{-2}$, specified HPA in DVB-S2(X).**

| ROF | Proposed algorithm | | | ACM $\beta = -5$dB | |
|---|---|---|---|---|---|
| $\gamma$ | Optimum IBO $\beta^{\dagger}$ (dB) | Optimum MODCOD | Spectrum efficiency | Optimum MODCOD | Spectrum efficiency |
| **0.05** | −3.145 | 16APSK-4/5 | 3.0149 | 16APSK-3/4 | 2.8255 |
| **0.10** | −3.38 | 16APSK-5/6 | 3.0002 | 16APSK-5/6 | 3.0002 |
| **0.15** | −3.03 | 16APSK-9/10 | 3.1020 | 16APSK-5/6 | 2.8697 |
| **0.20** | −3.19 | 16APSK-9/10 | 2.9728 | 16APSK-5/6 | 2.7502 |
| **0.25** | −2.63 | 16APSK-9/10 | 2.8539 | 16APSK-5/6 | 2.6401 |
| **0.35** | −2.375 | 16APSK-9/10 | 2.6425 | 16APSK-5/6 | 2.4446 |

the input BER $BER = 0.0348$, and the optimal combination of link parameters is $\{\ \alpha = \text{16APSK-5/6},\ \gamma = 0.10\ \}$.

The scheme proposed in this paper aims to optimize the SatCom link throughput by joint designing the IBO of non-linear PA, roll-off factor of RRC filters, as well as MODCOD conventionally used in current systems. This joint optimization is able to improve the link throughput. Here more information can be conveyed with the same bit rate since low order coding can be used. In this sense raw bit rate and bandwidth of the channel are not affected in our study, but the spectrum efficiency is improved.

It is worth mentioning that we study 16APSK modulation schemes as defined in the relevant the DVB-S2(X) standard as our paper is focused on SatCom systems. These systems presently rely on APSK simlations due to the favorable PAPR. When applying orthogonal frequency division multiplexing (OFDM), the signal PAPR will be determined by the modulation in each subcarrier and the number of subcarriers. The non-linear property is likely to have more profound effects not only in each subcarrier, but also across subcarriers. The investigation for the settings of this link will become more complicated, and this is a topic for future research, and will be reported separately.

## V. CONCLUSION

This paper first reported an equivalent full-linear link with additive noise, which can approximate the DVBS2(X) non-linear link with an HPA and RRC filters for BER analysis. Numerical and experimental results validated the equivalent linear link with additive noise source. Then, optimum HPA IBOs for different ROFs and channel noise power were obtained to minimize the system BER. With further consideration of the effects of different LDPC code rates to the BER performance and spectral efficiency, as well as the effects from different ROFs to the spectral efficiency, an adaptive operation algorithm to maximize the system spectrum efficiency while still guaranteeing the detection performance was formulated and validated.

## APPENDICES

The output signal power from the HPA is denoted as $P_{\text{out}}$. The BER is a $Q$-function related to the SNIR which is calculated as $SNIR = P_{\text{out}}/(\sigma^2_{\text{ISI}} + N_0)$, the increasing $SNIR$ can enhance the BER performance. Therefore, the target of the BER minimization can be transferred to the $SNIR$ maximization, i.e.

$$T_1 : \beta^{\dagger} = \arg\max_{\beta} \left[ P_{\text{out}} - (\sigma^2_{\text{ISI}} + N_0) \right] [\text{dB}]. \quad (17)$$

The definition of OBO is $\xi = P_{\text{out}} - P^{\text{sat}}_{\text{out}}$ [dB]. Therefore, the target $T_1$ could be rewritten as $T_2$:

$$T_2 : \beta^{\dagger} = \arg\max_{\beta} \left[ P^{\text{sat}}_{\text{out}} + \xi - (\sigma^2_{\text{ISI}} + N_0) \right] [\text{dB}]. \quad (18)$$

As the saturation output power $P^{\text{sat}}_{\text{out}}$ is a fixed value for a given HPA, $P^{\text{sat}}_{\text{out}}$ can be removed as

$$T_3 : \beta^{\dagger} = \arg\max_{\beta} \left[ \xi - (\sigma^2_{\text{ISI}} + N_0) \right] [\text{dB}]. \quad (19)$$

Next, the maximization is formulated as $T_4$

$$T_4 : \beta^{\dagger} = \arg\min_{\beta} \left[ -\xi + (\sigma^2_{\text{ISI}} + N_0) \right] [\text{dB}]. \quad (20)$$

With the consideration of ISI, the required SNRs for non-linear and linear systems are written as $\left[E_s/(N_0 + \sigma^2_{\text{ISI}})\right]^{\text{req}}_{\text{NL}}$ and $(E_s/N_0)^{\text{req}}_{\text{AWGN}}$, respectively, and in dB format, the relation between the two required SNRs is rewritten as

$$\left\{ (E_s)^{\text{req}}_{\text{NL}} - (N_0 + \sigma^2_{\text{ISI}}) \right\} [\text{dB}] = \left\{ (E_s)^{\text{req}}_{\text{AWGN}} - N_0 \right\} [\text{dB}], \quad (21)$$

and in dB format:

$$(N_0 + \sigma^2_{\text{ISI}})[\text{dBm}] = \left\{ (E_s)^{\text{req}}_{\text{NL}} + N_0 - (E_s)^{\text{req}}_{\text{AWGN}} \right\} [\text{dBm}]. \quad (22)$$

Note, the required $(E_s)^{\text{req}}_{\text{NL}}$ only considers the adverse impact from the ISI. Hence, the $(E_s)^{\text{req}}_{\text{NL}}$ is treated as the same value of $P_{out}$. Substituting (23) into (21) yields the optimization target as

$$\beta^{\dagger} = \min_{\beta} \left[ +(E_s)^{\text{req}}_{\text{NL}} - (E_s)^{\text{req}}_{\text{AWGN}} - \xi \right]. \quad (23)$$

As $N_0$ is independent of IBO, the final target is,

$$T_f : \beta^{\dagger} = \min_{\beta} \left\{ \left[ \frac{E_s}{N_0} \right]^{\text{NL}}_{\text{ref}} - \left[ \frac{E_s}{N_0} \right]^{\text{AWGN}}_{\text{ref}} - \xi \right\} [\text{dB}], \quad (24)$$

which is the definition of $D_{tot}$ in Section IV.A.

## REFERENCES

[1] *Evolution and Future of Broadband Satellite Services*, B. Price, ITU Satell. Symp., Geneva, Switzerland, Nov.28/30, 2018.
[2] J. Tronc, P. Angeletti, N. Song, M. Haardt, J. Arendt, and G. Gallinaro, "Overview and comparison of on-ground and on-board beamforming techniques in mobile satellite service applications," *Int. J. Satell. Commun. Netw.*, vol. 32, no. 4, pp. 291–308, Jul./Aug. 2014.
[3] D. G. Riccardo, A. Piero, P. Daniele, and R. Emiliano, "Future technologies for very high throughput satellite systems," *Int. J. Satell. Commun. Netw.*, vol. 38, no. 2, pp. 141–2161, Feb. 2020, Mar./Apr. 2020.
[4] N. Toptsidis, P.-D. Arapoglou, and M. Bertinelli, "Link adaptation for Ka band low earth orbit earth observation systems: A realistic performance assessment," *Int. J. Satellite Commun. Netw.*, vol. 30, pp. 131–146, May/Jun. 2012.
[5] W. Zhou, Y. Zhu, Y. Li, Q. Li, and Q. Yu, "Research on hierarchical architecture and routing of satellite constellation with IGSO-GEO-MEO network," *Int. J. Satell. Commun. Netw.*, vol. 38, no. 2, pp. 162–176, Mar. 2020.
[6] F. Massaro, M. Bergmann, R. Campo, M. Thiebaut, D. V. Finocchiaro, A. Arcidiacono, S. Eutelsat, G. Goussetis, J. Garcia-Perez, G. Amendola, and C. Riva, "QV-LIFT project: Using the Q/V band Aldo Paraboni demonstration payload for validating future satellite systems," in *Proc. 23rd Ka Broadband Commun. Conf.*, Trieste, Italy, Oct. 2017, pp. 1–16.
[7] X. Tian, G. Chen, K. Pham, and E. Blasch, "Joint transmission power control in transponded SATCOM systems," in *Proc. IEEE Mil. Commun. Conf. (MILCOM)*, Baltimore, MD, USA, Nov. 2016, pp. 126–131.
[8] *Digital Video Broadcasting (DVB); Second Generation Framing Structure, Channel Coding and Modulation Systems for Broadcasting, Interactive Services, News Gathering and Other Broadband Satellite Applications (DVB-S2)*, Standard ETSI EN 302 307 v1.2.1 (2009-08), 2009.
[9] R. D. Gaudenzi and R. Rinaldo, "Capacity analysis and system optimization for the reverse link of multi-beam satellite broadband systems exploiting adaptive coding and modulation," *Int. J. Satell. Commun. Netw.*, vol. 22, pp. 401–423, Jun. 2004.
[10] S. Cioni, R. De Gaudenzi, and R. Rinaldo, "Adaptive coding and modulation for the reverse link of broadband satellite networks," in *Proc. IEEE Global Telecommun. Conf. (GLOBECOM)*, Dallas, TX, USA, Nov./Dec. 2004, pp. 1101–1105.
[11] *Digital Video Broadcasting (DVB); Second Generation Framing Structure, Channel Coding and Modulation Systems for Broadcasting, Interactive Services, News Gathering and Other Broadband Satellite Applications; Part 2: DVB Extensions (DVB-S2X)*, Standard ETSI EN 302 307-2 v1.1.1 (2014-10), 2014.
[12] E. Casini, R. De Gaudenzin, and A. Ginesi, "DVB-S2 modem algorithms design and performance over typical satellite channels," *Int. J. Satell. Commun.*, vol. 22, pp. 281–318, 2004.
[13] J. Moron, R. Leblanc, P. Frijlink, F. Lecourt, M. Sigler, G. Goussetis, G. Amendola, G. Codispoti, G. Valente, and G. Parca, "A novel high-performance V-band GaN MMIC HPA for the QV-lift project," in *Proc. 24th Ka Broadband Commun. Conf.*, Niagara Falls, ON, Canada, 2018, pp. 1–6.
[14] E. G. Cabanillas, "Efficient non-linear ISI compensation techniques for commercial receivers," Netw. Internet Archit., Télécom Bretagne, Université de Bretagne Occidentale, Brest, France, 2014.
[15] T. J. Richardson and R. L. Urbanke, "The capacity of low-density parity-check codes under message-passing decoding," *IEEE Trans. Inf. Theory*, vol. 47, no. 2, pp. 599–618, Feb. 2001.
[16] L. Jordanova, L. Laskov, and D. Dobrev, "Influence of BCH and LDPC code parameters on the BER characteristic of satellite DVB channels," *Eng., Technol. Appl. Sci. Res.*, vol. 4, no. 1, pp. 591–595, Feb. 2014.
[17] M. W. Sun, M. C. Sanchez, A. Segneri, Y. Ding, S. McLaughlin, and G. Goussetis, "Optimising DVB-S2 (X) links in nonlinear environments," in *Proc. Microw. Technol. Techn. Workshop Conf.*, Noordwijk, The Netherlands, Feb. 2019, pp. 1–7.
[18] W. Sung, S. Kang, P. Kim, D.-I. Chang, and D.-J. Shin, "Performance analysis of APSK modulation for DVB-S2 transmission over nonlinear channels," *Int. J. Satell. Commun. Netw.*, vol. 27, no. 6, pp. 295–311, Nov. 2009.
[19] P. Chayratsami and S. Thuaykaew, "The optimum ring ratio of 16-APSK in LTE uplink over nonlinear system," in *Proc. 16th Int. Conf. Adv. Commun. Technol.*, Pyeongchang, South Korea, Feb. 2014, pp. 322–328.
[20] A. A. M. Saleh, "Frequency-independent and frequency-dependent nonlinear models of TWT amplifiers," *IEEE Trans. Commun.*, vol. COM-29, no. 11, pp. 1715–1720, Nov. 1981.
[21] G. Colavolpe, A. Modenini, and F. Rusek, "Channel shortening for nonlinear satellite channels," *IEEE Commun. Lett.*, vol. 16, no. 12, pp. 1929–1932, Dec. 2012.
[22] E. Cubukcu, "Root raised cosine (RRC) filters and pulse shaping in communication systems," NASA, May 2012.
[23] J. G. Proakis, *Digital Communications*, 4th ed. New York, NY, USA: McGraw-Hill, 2001, ch. 9.
[24] K. Mukumoto and T. Wada, "Realization of root raised cosine roll-off filters using a recursive FIR filter structure," *IEEE Trans. Commun.*, vol. 62, no. 7, pp. 2456–2464, Jul. 2014.
[25] J.-A. Lucciardi, N. Thomas, M.-L. Boucheret, C. Poulliat, and G. Mesnager, "Trade-off between spectral efficiency increase and PAPR reduction when using FTN signaling: Impact of non linearities," in *Proc. IEEE Int. Conf. Commun. (ICC)*, May 2016, pp. 1–7.
[26] K. Gentile, *Digital Pulse-Shaping Filter Basics*. Norwood, MA, USA, Analog Devices, 2007.
[27] A. A. M. Saleh and J. Salz, "Adaptive linearization of power amplifiers in digital radio systems," *Bell Syst. Tech. J.*, vol. 62, no. 4, pp. 1019–1033, Apr. 1983.
[28] R. Piazza, B. S. M. R., and B. Ottersten, "Multi-gateway data predistortion for non-linear satellite channels," *IEEE Trans. Commun.*, vol. 63, no. 10, pp. 3789–3802, Oct. 2015.
[29] T. Gotthans, R. Marsalek, J. Kral, and T. Urbanec, "Linearity and efficiency enhancement techniques for satellite communications," in *Proc. IEEE Topical Conf. RF/Microwave Power Model. Radio Wireless Appl. (PAWR)*, Jan. 2022, pp. 54–57.
[30] M. J. C. Sanchez, A. Segneri, S. A. Kosmopoulos, Q. Zhu, T. A. Tsiftsis, A. Georgiadis, and G. Goussetis, "Novel data pre-distorter for APSK signals in solid-state power amplifiers," *IEEE Trans. Circuits Syst. I, Reg. Papers*, vol. 66, no. 10, pp. 4044–4054, Oct. 2019.
[31] S. Meza, M. O'Droma, Y. Lei, and A. Goacher, "Some new memoryless behavioural models of wireless transmitter solid state power amplifiers," in *Proc. IEEE Int. Conf. Autom., Quality Test., Robot.*, May 2008, pp. 96–98.
[32] V. Vijayarangan and R. Sukanesh, "An overview of techniques for reducing peak to average power ratio and its selection criteria for orthogonal frequency division multiplexing radio systems," *J. Theor. Appl. Inf. Technol.*, vol. 5, no. 1, pp. 25–36, 2009.
[33] P. Chayratsami and S. Thuaykaew, "The optimum ring ratio of 16-APSK in LTE uplink over nonlinear system," in *Proc. 16th Int. Conf. Adv. Commun. Technol.*, Feb. 2014, pp. 805–809.

**MENGWEI SUN** (Member, IEEE) received the Ph.D. degree from the School of Information and Communication Engineering, Beijing University of Posts and Telecommunications (BUPT), in 2017.

She is currently a Research Associate with the School of Engineering, The University of Edinburgh, Edinburgh, U.K. Prior to this, she is a Research Associate with the Institute of Sensors, Signals and Systems (ISSS), Heriot-Watt University, Edinburgh. She received the Outstanding Doctoral Candidate of Universities, Beijing, in 2017, and the Excellent Doctoral Dissertation of SICE Department, BUPT, in 2017. Her research interests include Bayesian inference in modular and distributed sensor networks, and signal processing for wireless communications.

**GEORGE GOUSSETIS** (Senior Member, IEEE) received the Diploma degree in electrical and computer engineering from the National Technical University of Athens, Athens, Greece, in 1998, the B.Sc. degree (Hons.) in physics from the University College London, London, U.K., in 2002, and the Ph.D. degree from the University of Westminster, London, in 2002.

In 1998, he joined Space Engineering, Rome, Italy, as an RF Engineer. He was a Research Assistant with the Wireless Communications Research Group, University of Westminster, in 1999. From 2002 to 2006, he was a Senior Research Fellow with Loughborough University, Loughborough, U.K. He was a Lecturer (Assistant Professor) with Heriot-Watt University, Edinburgh, U.K., from 2006 to 2009, and a Reader (Associate Professor) with Queen's University Belfast, Belfast, U.K., from 2009 to 2013. He joined Heriot-Watt University, as a Reader, in 2013, and was promoted to a Professor, in 2014. He is currently the Head of the Institute of Sensors, Signals and Systems (ISSS), Heriot-Watt University. His research interests include the modelling and design of microwave filters, frequency-selective surfaces and periodic structures, leaky wave antennas, microwave sensing and curing as well numerical techniques for electromagnetics.

**KAI XU** is currently pursuing the Ph.D. degree with Heriot-Watt University and The University of Edinburgh. His current research interests include backscattering communication, hybrid beamforming network for massive MIMO systems, analysis and design of antennas, and communications security.

**YUAN DING** (Member, IEEE) received the bachelor's degree in electronic engineering from Beihang University (BUAA), Beijing, China, in 2004, the master's degree in electronic engineering from Tsinghua University, Beijing, in 2007, and the Ph.D. degree in electronic engineering from the Queen's University of Belfast, Belfast, U.K., in 2014.

He is currently an Assistant Professor with the Institute of Sensors, Signals and Systems (ISSS), Heriot-Watt University, Edinburgh, U.K. His research interests include the IoT-related physical-layer designs, antenna array, physical layer security, and 5G related areas.

**STEPHEN MCLAUGHLIN** (Fellow, IEEE) received the B.Sc. degree from the University of Glasgow, in 1981, and the Ph.D. degree from The University of Edinburgh, in 1990.

From 1981 to 1986, he was a Development Engineer in industry. In 1986, he joined the Department of Electronics and Electrical Engineering, The University of Edinburgh, and ultimately held a Chair in electronic communication systems. In October 2011, he joined Heriot-Watt University, as a Professor of signal processing. He is currently the Head of the School of Engineering and Physical Sciences, Heriot-Watt University, Edinburgh, U.K. He is a fellow of the Royal Academy of Engineering, the Royal Society of Edinburgh, and the Institute of Engineering and Technology. He is a EURASIP Fellow.

**ANDREA SEGNERI** received the B.Sc. degree in mathematics, the M.Sc. degree in applied mathematics, and the B.Sc. degree in civil and industrial engineering from the Sapienza University of Rome, Italy, in 2009, 2012, and 2016, respectively. He is currently pursuing the Ph.D. degree with Heriot-Watt University, Edinburgh, U.K.

From 2012 to 2014, he worked on a research and development project adopting fiber Bragg grating sensors for an Italian company. Since 2016, he has been with Step Over Srl, an Italian S.M.E. involved in many projects in the space and telecommunication sector, such as the software development of satellite payload management and reconfiguration modules. His research interest includes modeling end-to-end satellite communication systems supporting digital interference mitigation techniques.

**MARÍA JESÚS CAÑEVATE SÁNCHEZ** received the B.Eng. degree (Hons.) in telecommunication systems engineering from the Technical University of Cartagena, Cartagena, in 2014, and the Ph.D. degree in electrical engineering from Heriot-Watt University, Edinburgh, U.K., in 2018.

Her Ph.D. work was partly funded by the company Space Engineering (SPEN), now part of the world leading Airbus Defence and Space, Space Systems, where she stayed while pursuing the Ph.D. degree, in 2015. In 2018, she received an International Mobility Grant to stay at the company MBI Srl, Pisa, Italy, to collaborate in the European Project Q/V-band Earth Segment Link for Future High Throughput Space Systems. Her main research interests include power amplifier behavioral modeling and non-linear analysis of RF signals for end-to-end communication system performance evaluation.